Available online at www.sciencedirect.com
ScienceDirect
Polymer 47 (2006) 7506–7518
polymer
www.elsevier.com/locate/polymer

The influence of temperature and strain rate on the constitutive and damage responses of polychlorotrifluoroethylene (PCTFE, Kel-F 81)

Eric N. Brown [a,*], Philip J. Rae [a], E. Bruce Orler [b]

[a] *Materials Science and Technology Division, Structure/Property Relations, Los Alamos National Laboratory, MS G755, Los Alamos, NM 87545, USA*
[b] *Materials Science and Technology Division, Polymers & Coatings, Los Alamos National Laboratory, MS E549, Los Alamos, NM 87545, USA*

Received 11 July 2006; received in revised form 15 August 2006; accepted 16 August 2006
Available online 11 September 2006

Abstract

Polychlorotrifluoroethylene (PCTFE), also known as Kel-F 81, is a semi-crystalline fluoropolymer. Although it has been employed in a wide range of cryogenic components, valve seats, seals, and microelectronics packaging, its mechanical behavior has received limited coverage in the literature. In this work, we present the tensile and compressive constitutive response of PCTFE for a range of temperatures (−85 to 150 °C) and strain rates (1×10^{-4}–2.9×10^{3} s^{-1}). Both large-strain experiments based on flow stress and small-strain dynamic mechanical analysis (DMA) using the elastic modulus exhibit a strong increase in the glass transition temperature, T_g, with increasing strain rate. The quasistatic fracture behavior of PCTFE is presented using *J*-integral fracture experiments. Finally, a discussion of the implication of the constitutive and damage responses of PCTFE on impact failure modes observed in Taylor impact experiments is presented.

Keywords: Polychlorotrifluoroethylene (PCTFE); Constitutive response; Taylor impact

1. Introduction

Polychlorotrifluoroethylene (PCTFE) is a fluoropolymer closely related in chemical structure to the more common polytetrafluoroethylene (PTFE) and shares many similarities in ductile mechanical characteristics. Notably, however, the replacement of one out of every four fluorine atoms along the carbon backbone with a larger chlorine atom prevents the crystalline phase transitions that dominate the mechanical response of PTFE (see Refs. [1–14]). A common trade name for PCTFE as manufactured by the 3M company is Kel-F 81. It is melt processable, resistant to most common chemicals, highly electrically insulating and extremely impervious to water absorption. The most common industrial uses are for cryogenic components, valve seats, seals, and microelectronics packaging. As such, while the literature contains numerous studies on adhesive properties of PCTFE (see for example Refs. [15–19]), there is limited information on the mechanical or failure behavior of bulk PCTFE. McCrum [20,21] performed early dynamic mechanical analysis (DMA) studies to investigate the effects of temperature and crystallinity on the small-strain behavior of PCTFE, and a limited number of authors have studied the effect of temperature on the tensile response of PCTFE [22–25]. A brief study of PCTFE failure surfaces employing low resolution scanning electron microscopy has been presented by Shoemaker and Sterling [26]. The crystal structure is reported by Mencik [27] and the glass transition temperature is investigated by Hoffman (T_g = 52 °C), Privalko (T_g = 64 °C), Khanna (T_g = 75 °C), and Chang (T_g = 47–77 °C depending on crystallinity) [28–31]. The shock response of PCTFE has been reported by Marsh, Anderson and Sheffield [32–34]. The pressure and temperature dependences of the dielectric and ultrasonic properties of PCTFE have been detailed by Samara and Fritz [35].

* Corresponding author. Tel.: +1 505 667 0799; fax: +1 505 667 2185.
E-mail address: en_brown@lanl.gov (E.N. Brown).

0032-3861/$ - see front matter © 2006 Elsevier Ltd. All rights reserved.
doi:10.1016/j.polymer.2006.08.032

A motivation for this research was to investigate the relationship between this material and a copolymer of PCTFE and polyvinylidene fluoride (PVDF) called Kel-F 800. The copolymer was also manufactured by the 3M company, consisting of 75 mol% PCTFE and 25 mol% PVDF. However, the introduction of PVDF into the copolymer dramatically changes the crystallinity, the glass transition temperature, and the mechanical response. As such, direct comparison between Kel-F 81 and Kel-F 800 offers limited insight. An extensive investigation of the influence of temperature and strain rate on the constitutive and damage responses of Kel-F 800 will be presented in a subsequent publication. Nevertheless, the current investigation of PCTFE presents a number of unique features of importance to the mechanical response of the homopolymer.

In the current work the constitutive response of PCTFE is presented in both tension and compression to large strains. The compressive response is presented for a temperature ranging from −85 to 150 °C and strain rates of 1×10^{-4}–$2.9 \times 10^{3}\ s^{-1}$. The tensile response is reported for a temperature ranging from −50 to 100 °C and strain rates of 1.1×10^{-4}–$1.1 \times 10^{-1}\ s^{-1}$. Yield behavior in tension is coupled with necking in the gage section. At temperatures of 23 °C and above the neck is subsequently drawn out, whereas at lower temperature the neck localizes leading to the prompt failure. Both the large-strain experiments based on flow stress and small-strain dynamic mechanical analysis (DMA) using the elastic modulus exhibit a strong increase in the glass transition temperature, T_g, with increasing strain rate. The quasistatic fracture behavior of PCTFE is presented using J-integral fracture experiments. Below T_g, the fracture toughness of PCTFE has a relatively low temperature dependence, but above T_g the increased ductility results in a significant increase in J_{IC} around 65 °C followed by a precipitous drop in toughness. A discussion of the implication of the constitutive and damage responses of PCTFE on impact failure modes observed in Taylor impact experiments is presented.

2. Experimental procedure

2.1. Material and sample preparation

A PCTFE billet of compression molded Neoflon® measuring $500 \times 500 \times 25\ mm^3$ was purchased for investigation in this study. The molding powder used is manufactured by Daikin Industries of Japan. The crystallinity was estimated from the differential scanning calorimetry (DSC) melt endotherm obtained in a TA Instruments Q1000, Fig. 1. Measurement of the melt peak in PCTFE determined a release of ΔH_f^{sample} equal to $19.9\ J\,g^{-1}$. Crystallinity was calculated as $X_C = \Delta H_f^{sample}/\Delta H_f^0$ using the literature value for ΔH_f^0 of $43.5\ J\,g^{-1}$ [36], which suggests a crystallinity of 46%. Other references suggested slightly different value for ΔH_f^0 of $43.2\ J\,g^{-1}$ [37] and $41.9\ J\,g^{-1}$ [38]. The use of both of these slightly lower estimates would result in higher crystallinity estimates. The density was measured by helium pycnometry and

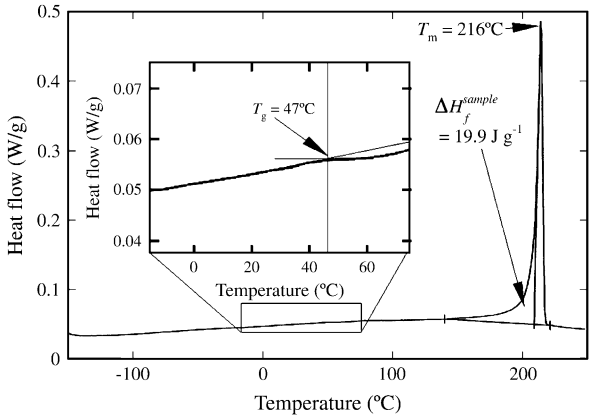

Fig. 1. DSC scan of PCTFE.

was found to be $2158 \pm 1\ kg\,m^{-3}$. Following the equation proposed by Hoffman and Weeks [28] this implies a crystallinity of 75%.[1] Different methods of measuring crystallinity have been compared by Murthy et al. [39]. The glass transition temperature, T_g, was measured to be 47 °C, from a very subtle endotherm in the DSC trace. The DSC melt peak temperature was 216 °C at $10\ °C\,min^{-1}$. Specimens were machined from the pressed and sintered billets of pedigreed PCTFE while ensuring a nominal temperature rise to prevent changes in the material's crystallinity.

2.2. Compression and tension

Given the ductile nature of PCTFE, large-strain deformations were investigated. For this reason, all strains referenced in this paper, unless otherwise noted, are true-strains (logarithmic strains). A constant true strain rate was maintained for all large-strain compression experiments. The feedback loop from the testing machines was closed to correctly slow the crosshead speed as the samples thinned. True-stress was calculated assuming a constant sample volume. The compression sample geometry chosen was 6.375 mm diameter by 6.375 mm long right-regular cylinders. The aspect ratio of 1:1 is smaller than the 1:1.5–1:2 values often employed in compression tests on metals, but the sample size and ratio were chosen to conserve material for the large number of tests required and prevent the trapezoidal shearing deformation mode observed in some soft polymers.

For the compression tests both MTS 880 and MTS 810 servo-hydraulic machines were utilized. These machines ran MTS TestStar software allowing for full control over the test

[1] As previously discussed for PTFE [2,3,5] density methods routinely report higher values of crystallinity than DSC. This is due to the partitioning by the density method of oriented domains but not thermodynamically crystalline domains of crystalline material, which is not included by DSC. Moreover, Hoffman and Weeks [28] used an immersion method to measure density as opposed to helium pycnometry. While the different methods generate different values for crystallinity, they are highly repeatable, provide meaningful comparison between studies as long as the technique for quantifying crystallinity is kept constant, and the different techniques similarly capture crystallinity changes due to thermal processing.

profile. In all samples tested at −20 °C, or higher, paraffin wax was used to lubricate the specimen ends [40–42]. The specimens were compressed between highly polished tungsten carbide platens to further reduce frictional effects. Temperature control was carried out using either electrically heated or liquid nitrogen cooled platens and surrounding insulation was used to create a small environmental chamber. The samples were allowed to equilibrate at temperature between 30 and 45 min prior to testing.

For the tensile experiments, a screw driven Instron 4482 frame was used. This machine has been fitted with a modern PC control system (MTS Testworks 4) allowing a wide range of control modes and input channels. Samples were machined to form ASTM D-638 Type V specimens. All specimens were allowed to equilibrate at the testing temperature between 45 and 100 min prior to tensile testing. Following a linear elastic loading, a load drop was observed to occur coincident with the formation of a neck. Upon necking the sample is no longer in a uniaxial stress state and the data generated are essentially invalid except to verify predictions from a full three-dimensional computer model. To obtain accurate data on the uniaxial part of the curve, an Instron 2620 extensometer was utilized. This had a gage length of 9.20 mm and a maximum displacement of 5.08 mm, leading to a maximum sample true strain of 0.44. Since, in tension, valid data are only obtained for strains less than 8% due to the onset of necking, plots are made between engineering stress and strain to indicate the loss of uniaxial loading. At such low strains before the necking point, true and engineering values are essentially identical.

For high strain-rate compression testing ($2900 \pm 100\ s^{-1}$), a split-Hopkinson pressure bar (SHPB) was used [43]. This Hopkinson bar is fitted with a small environmental chamber surrounding the test sample. In the chamber, either heated or cooled gas can be introduced to vary the sample temperature between −100 and 200 °C. The change in impedance at the ends of the Ti–6Al–4V bars used for testing in this temperature range is negligible. As before, paraffin wax was used to lubricate the specimen ends for all samples tested at −20 °C or higher. No lubricant was used at lower temperatures, but owing to the relatively small strains imposed on the sample and the low coefficient of friction between PCTFE and the finely finished pressure bars, no sample barreling was found.

2.3. Ultrasonic sound speed measurements

The speed of sound in PCTFE was measured using a time of flight method [44]. A Panametrics 5077PR pulser/receiver was paired with Panametrics V155 and V109 transducers. Timing was obtained from a Tektronix TDS 754D oscilloscope. Room temperature samples of 12 mm thick were tested using longitudinal (C_l) and shear wave (C_s) inducing heads. Measurements were suitably corrected for triggering and coupling medium delays. Values for Young's modulus (E), Poisson's ratio (ν), shear modulus (G), and bulk modulus (K) at minute strains are obtained using the material density (ρ) and the following expressions:

$$\nu = \frac{C_l^2 - 2C_s^2}{2\left(C_l^2 - C_s^2\right)}, \tag{1}$$

$$E = 2\rho C_s^2(1+\nu), \tag{2}$$

$$G = \frac{E}{2(1+\nu)}, \tag{3}$$

$$K = \frac{E}{3(1-2\nu)}. \tag{4}$$

2.4. Dynamic mechanical analysis (DMA)

The in-phase elastic (storage) shear modulus G' and loss modulus G'' were measured as a function of temperature and frequency by DMA. The loss factor, $\tan\delta$, was calculated as G''/G'. Torsional geometry samples were analyzed using a TA Instruments ARES with 2 kg force rebalance transducer. Sample bars were machined to 1.5 mm thick by 10 mm wide and 15 mm long. Frequency/temperature sweeps were obtained from 0.1 to 100 rad s^{-1} at 0.1% strain under a nitrogen purge from −125 °C to melt (~216 °C).

2.5. J-integral fracture toughness

Fracture toughness measurements were performed using compact tension (1/2CT) specimens as previously presented by Brown and Dattelbaum [5]. The test geometry, as defined in ASTM Standard E-1820-01, is modified to enable a crack opening displacement (COD) gage to be mounted along the loading line. The specimen notch was cut to have an inclusive angle of 40°, which was subsequently sharpened with a razor blade according to ASTM Standard D-5045. Tests were performed using an MTS 880 load frame under constant cross-head displacement rates of 0.025 mm s^{-1}. Load–line displacements were measured with an MTS COD gage 632.03E-31. Tests were performed at −50, −15, 23, 40, 70, and 80 °C using an MTS 612 environmental chamber. J-integral values corresponding to the ith data pair are given by

$$J_i = J_{el_i} + J_{pl_i} = \frac{K_i^2(1-\nu^2)}{E} + \frac{\eta_{pl}A_i^{pl}}{b(w-a_0)}, \tag{5}$$

where J_{el} and J_{pl} signify the division of energy into recoverable elastic deformation and permanent plastic deformation, respectively. The linear–elastic stress intensity factor K_i for a specimen with a crack length of a_i is calculated according to ASTM Standard E-1820-01. The Poisson's ratio, ν, is taken to be 0.39, E is the Young's modulus, $\eta_{pl} = 2 + 0.522(w - a_{bi})/w$ is a dimensionless constant ($a_{bi} = a_0 + J_i/2\sigma_{ys}$ is the blunting corrected crack length that corresponds to the ith data point), A_i^{pl} is the area under the load displacement curve, and a_0 is the initial crack length. The width, w, and the thickness, b, of the specimen are nominally 39.8 mm and 19.1 mm, respectively. The initial tangent modulus and

Table 1
Mechanical properties for PCTFE in tension as a function of temperature

Temperature (°C)	Tangent modulus (GPa)	2% Yield stress (MPa)
−50	2.72	80.2
−15	2.20	62.5
23	1.72	38.6
40	1.53	31.0
70	0.92	16.7
80	0.72	13.3

2% offset yield stress values used in this work are given in Table 1 in the results section. To rigorously evaluate J_{IC} during stable crack propagation $J-R$ curve data are constructed with the critical fracture criterion, J_{IC}, defined as the fracture toughness of the material at fracture instability prior to the onset of significant stable crack extension (the point of 0.2 mm of crack growth beyond crack tip blunting) through the normalization technique. The normalization technique was proposed by Landes and Herrera [45] and has been included in ASTM Standard E-1820 for elastic–plastic fracture toughness. Although developed for metals, the normalization technique has been demonstrated to yield equivalent results to multi-specimen methods for a variety of polymers [46–48]. This method, as presented in full by Brown and Dattelbaum [5], uses an analytical solution with power-law behavior for blunting and initiation, and smoothly undergoes transitions to a linear relationship for steady state crack growth thus giving an accurate estimate of the crack tip position over the course of the test.

Fracture surface morphologies were examined with a JEOL JSM–6300FXV scanning electron microscope (SEM). After fracture, specimens were notched along the centerline from the backside and subsequently immersed in liquid nitrogen for approximately 30 min. Samples were immediately reloaded to propagate a brittle crack from the arrested crack tip. Areas of interests were then dissected, mounted, and sputtered with carbon to promote electrical conductivity thus reducing charging. Micrographs were obtained using 5 keV secondary electrons.

2.6. Taylor impact

The Taylor test involves propelling a right cylindrical specimen with high length over diameter ratio at a velocity on the order of hundreds of m s^{-1} against an ''infinite'' steel block. Although originally developed as a method of estimating the dynamic yield strength of metals, it is now mostly used as a verification for a computational computer codes' predications of dynamic material response. We have previously had great success in using the Taylor test to study the temperature and rate dependences of the dynamic ductile-to-brittle transition in PTFE [4], which we extend here for PCTFE. Taylor cylinders were machined with dimensions of 7.62 mm diameter by 38.1 mm long. Rods were fired at velocities between 105 and 202 m s^{-1} and temperatures of 23 and 60 °C. An Imacon 200 high-speed framing camera coupled to a Cordin 463 proportional delay generator was used to record backlit images of the impacts. In all cases a 350 ns exposure was used and 16 frames were recorded with 15 μs inter-frame time. Rae et al. [4] provide a complete description of the experimental setup employed.

3. Results

3.1. Compression and tension

Fig. 2 shows the compressive response of PCTFE as a function of strain rate. At lower rates, the response is seen to be nearly elastic–perfectly plastic while at higher rates a significant yield drop is seen. At rates of 10 and 100 s^{-1} a post-yield drop in stress was observed followed by significant strain hardening above 30% true strain. As expected for a ductile polymer such as PCTFE, all samples were capable of accommodating a deformation to 50% true strain without evidence of cracking or failure. Consistent with most polymers, the flow stress exhibits strong rate dependence. At rates up to 1 s^{-1}, the cross-head direction was reversed to generate unloading data. This was not possible at the higher rates because of instrument inertia, although the samples were recovered intact.

The compressive response as a function of temperature is shown in Fig. 3. It can be seen that the yield strength is highly

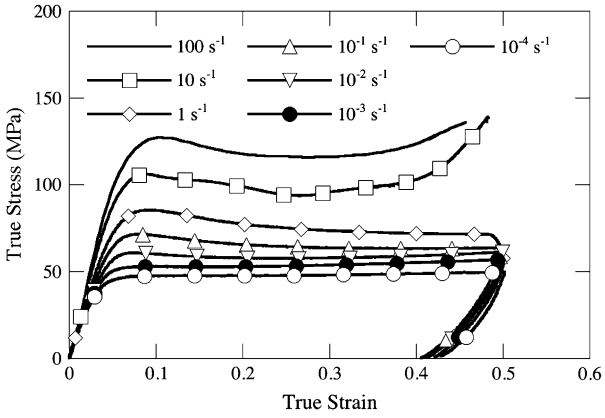

Fig. 2. The effect of strain rate on the compressive response of PCTFE at 23 °C.

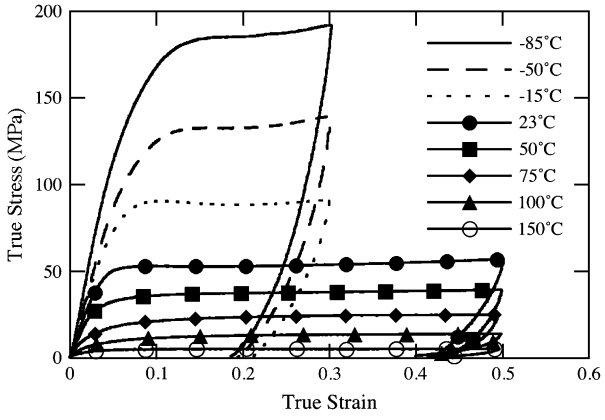

Fig. 3. The effect of temperature on the compressive response of PCTFE at 10^{-3} s^{-1}.

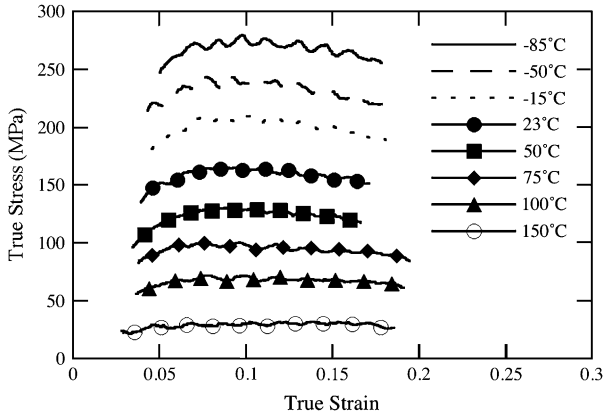

Fig. 4. The SHPB high strain rate ($2900 \pm 100\ s^{-1}$) compressive properties of PCTFE as a function of temperature.

dependent on temperature. Although the loading modulus is higher for lower temperatures, the increase in yield stress is more dominant leading to associated increases in yield strain. Above T_g, the yield stress becomes harder to define and more of a gentle rolling over in the stress–strain curve is observed. In view of the lower ductility of polymers at cold temperatures, samples at or below room temperature were only loaded to 30% true strain. Additionally, it can be seen that strain hardening is almost absent and independent of temperature above −15 °C.

The higher rate, split-Hopkinson pressure bar, compressive response is shown in Fig. 4. The initial parts of the curves are not shown since the specimens were not in dynamic equilibrium. Below T_g, a peak stress is reached followed by a yield drop similar to the results at lower rates (10 and $100\ s^{-1}$). Above T_g, however, a uniform flow stress is observed. The flow stress is highly dependent on temperature.

The tensile response as a function of four strain rates is shown in Fig. 5. The range of rates is not as extensive as in compression, however, a significant strain-rate effect is observed. At a comparable rate of $\sim 1 \times 10^{-3}\ s^{-1}$ the room temperature yield in compression is 53 MPa while in tension

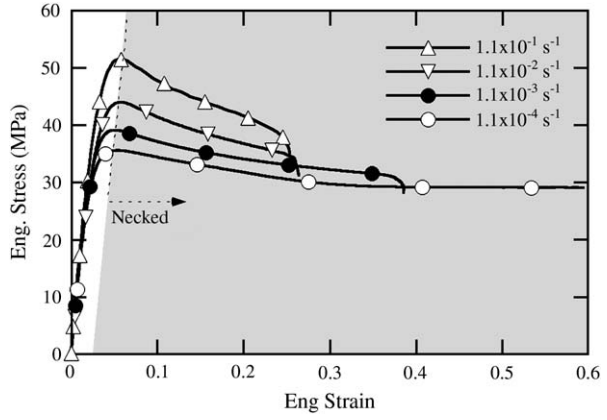

Fig. 5. The effect of strain rate on the tensile response of PCTFE at 23 °C. Note: the material necked immediately after yielding leading to a triaxial stress state after ~5–6% strain.

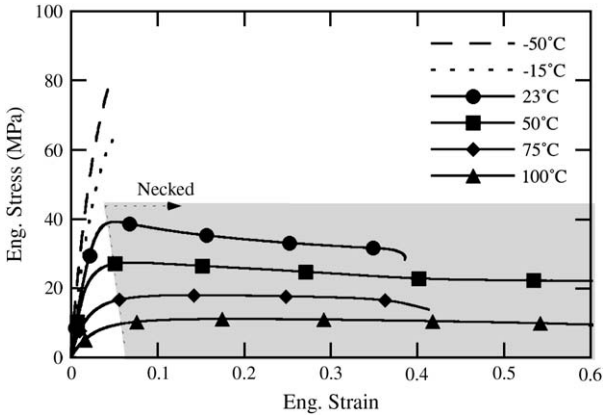

Fig. 6. The effect of temperature on the tensile response of PCTFE at $1.1 \times 10^{-3}\ s^{-1}$. Note: the material necked immediately after yielding at 23 °C and above leading to a triaxial stress state after ~5–6% strain.

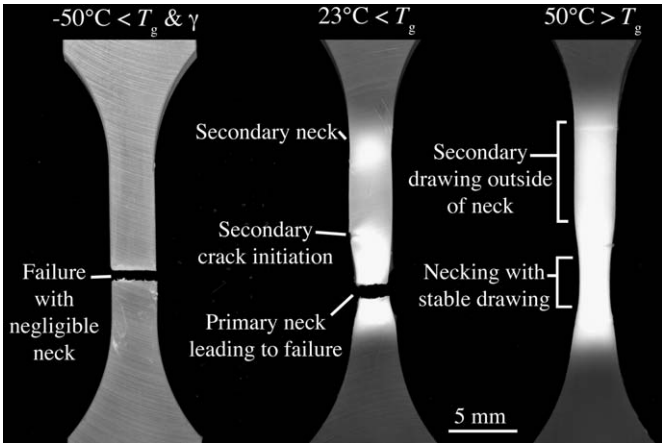

Fig. 7. Tensile failure modes with varying degrees of necking as a function of temperature.

it is 39 MPa, a 26% reduction. After yielding in tension, all specimens necked and formed localized failure points. Thus a triaxial stress state was created invalidating the uniaxial stress assumption.

Fig. 6 shows the tensile response as a function of temperature. At −15 °C the sample failed just after yielding. At −50 °C the sample failed before any apparent yield, as shown in Fig. 7. The lack of necking or strain whitening corresponds to temperature below the γ transition[2] in PCTFE, which is discussed more later. At room temperature and above, the sample necked leading to localized failure. At temperatures above T_g, the neck region was larger than below T_g and showed some evidence of the onset of drawing. As in compression, the loading modulus up to yield is larger at lower temperatures and the yield stress becomes ill-defined above T_g. The mechanical

[2] McCrum et al. [51] present a discussion of the α, β, and γ transitions in PCTFE. The α transition is reported to be a very subtle peak that is only present in very high crystalline material. The dominant peaks are the β (associated with the T_g) and γ transitions.

properties for PCTFE in tension as a function of temperature are given in Table 1.

3.2. Ultrasonic sound speed measurements

Values of Young's modulus, Poisson's ratio, shear modulus, and bulk modulus calculated using the sound speeds are shown in Table 2. Application of Eqs. (1–4) assumes the material is isotropic and that in the range of the minute imposed strains the material behaves in a linear elastic manner. The values reported are similar to those found in the literature, shown in Table 3.

3.3. Dynamic mechanical analysis (DMA)

Dynamic mechanical analysis was performed to measure the small-strain elastic and viscous response of PCTFE over a wide temperature range. The frequency was varied from 0.1 to 100 rad s^{-1}. The results of DMA scans run at four deformation rates are shown in Fig. 8. The tan δ curves exhibit a dependence of T_g on deformation frequency, varying from approximately 76 to 104 °C. The breaks in the gradient of G', indicating T_g, occur at 63–79 °C indicating that the initial deviancy temperature is less dependent on frequency. The behavior is consistent with the earlier results of McCrum [20,21]. The small-strain shear elastic response values from DMA are compared to the large deformation tangent modulus (Young's modulus) data by employing Eq. (3) and using the ultrasound measured Poisson's ratio, $\nu = 0.39$. Keeping in mind that for Eq. (3) to hold rigorously for relating G and E, the assumptions of classic isotropic homogeneous linear elasticity must be valid. While PCTFE is semi-crystalline, the shear modulus data acquired by DMA and Young's modulus data acquired by tensile dog-bone tests are in agreement quantitatively (Fig. 8). Error bars for the tensile data fall within the data points. In addition to the rate dependence of T_g (also referred to as the β transition), it is worth noting that the γ transition exhibits a similar rate dependence varying from approximately −60 to −10 °C.

Table 2
Ultrasonic wave-speeds and calculated elastic constants

Property	Value
Longitudinal wave speed, C_l	1870 ± 10 m s^{-1}
Shear wave speed, C_s	780 ± 10 m s^{-1}
Density, ρ	2158 ± 1 kg m^{-3}
Young's modulus, E	3.66 GPa
Shear modulus, G	1.31 GPa
Bulk modulus, K	5.80 GPa
Poisson's ratio, ν	0.39

Table 3
Literature sound speed and density values for PCTFE

Longitudinal wave speed, C_l (m s^{-1})	Shear wave speed, C_s (m s^{-1})	Density, ρ (kg m^{-3})	Source
1890	750	2140	Dick et al. [52]
1850	~780 (extrapolated)	~2140 (extrapolated)	Kwan et al. [53]
1740	770	2122	Marsh [32]

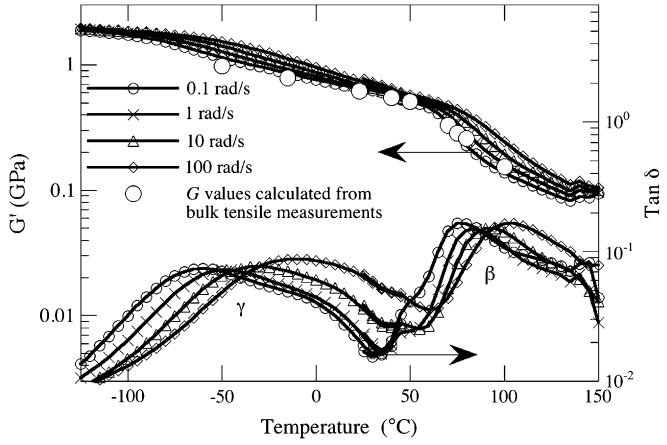

Fig. 8. The results of a DMA scan run at four deformation rates.

Quasistatic (0.025 mm s^{-1}) load–displacement curves for PCTFE compact tension samples are shown in Fig. 9 at

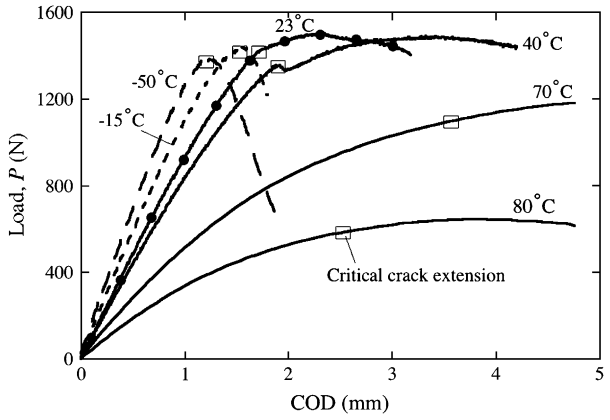

Fig. 9. Representative load–displacement curves at a displacement rate of 0.025 mm s^{-1} as a function of temperature.

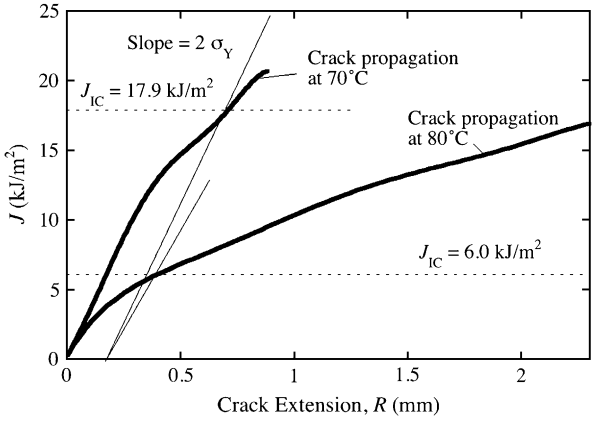

Fig. 10. Representative J–R curves obtained using the normalization technique corresponding to 70 and 80 °C.

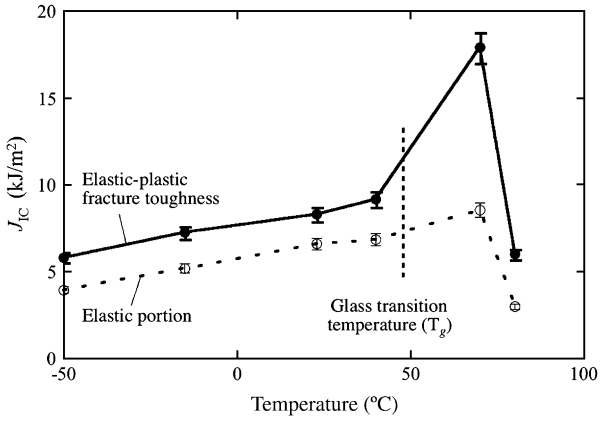

Fig. 11. Fracture toughness values, J_{IC}, at a displacement rate of 0.025 mm s^{-1} as a function of temperature.

−50, −15, 23, 40, 70, and 80 °C. Samples were maintained at testing temperature for a minimum of 60 min to ensure thermal equilibrium. At all temperatures considered, PCTFE behaves nonlinearly requiring the full J-integral fracture toughness analysis. Below T_g, the load–displacement records provide clear indications for initiation of crack propagation from peak-load and pop-in criteria. Above T_g, the onset of crack propagation is much more subtle. Thus the critical value of J can only be determined from J–R curves, shown in Fig. 10. The dependence of J_{IC} on temperature is shown in Fig. 11. Below the glass transition temperature the plastic contribution to J_{IC} remains constant and J_{IC} increases slightly with temperature. Immediately above the glass transition temperature the plastic contribution increases significantly due to increased ductility, while the elastic contribution follows the same trend as below T_g. The combined effect doubles the fracture toughness immediately above T_g. A further increase in temperature, however, causes a subsequent dramatic decrease in the fracture toughness.

Changes in the fracture mechanisms of PCTFE associated with the glass transition temperature are elucidated by the investigation of the fracture plane morphology. Two major mechanisms are observed in the scanning electron

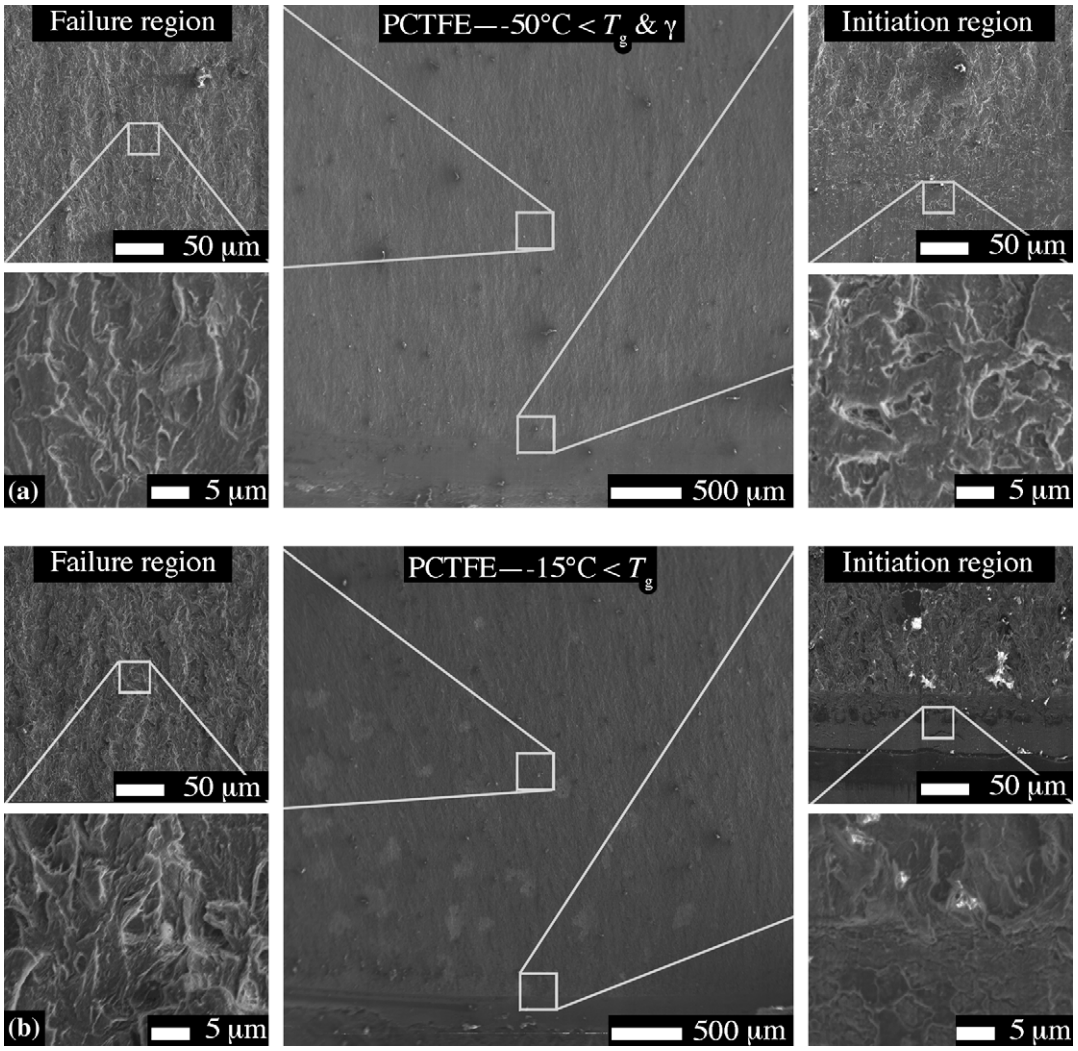

Fig. 12. SEM micrographs of the fracture plane morphology for PCTFE below the glass transition temperature at 0.025 mm s^{-1} loading rate. Note: crack propagation is from bottom to top.

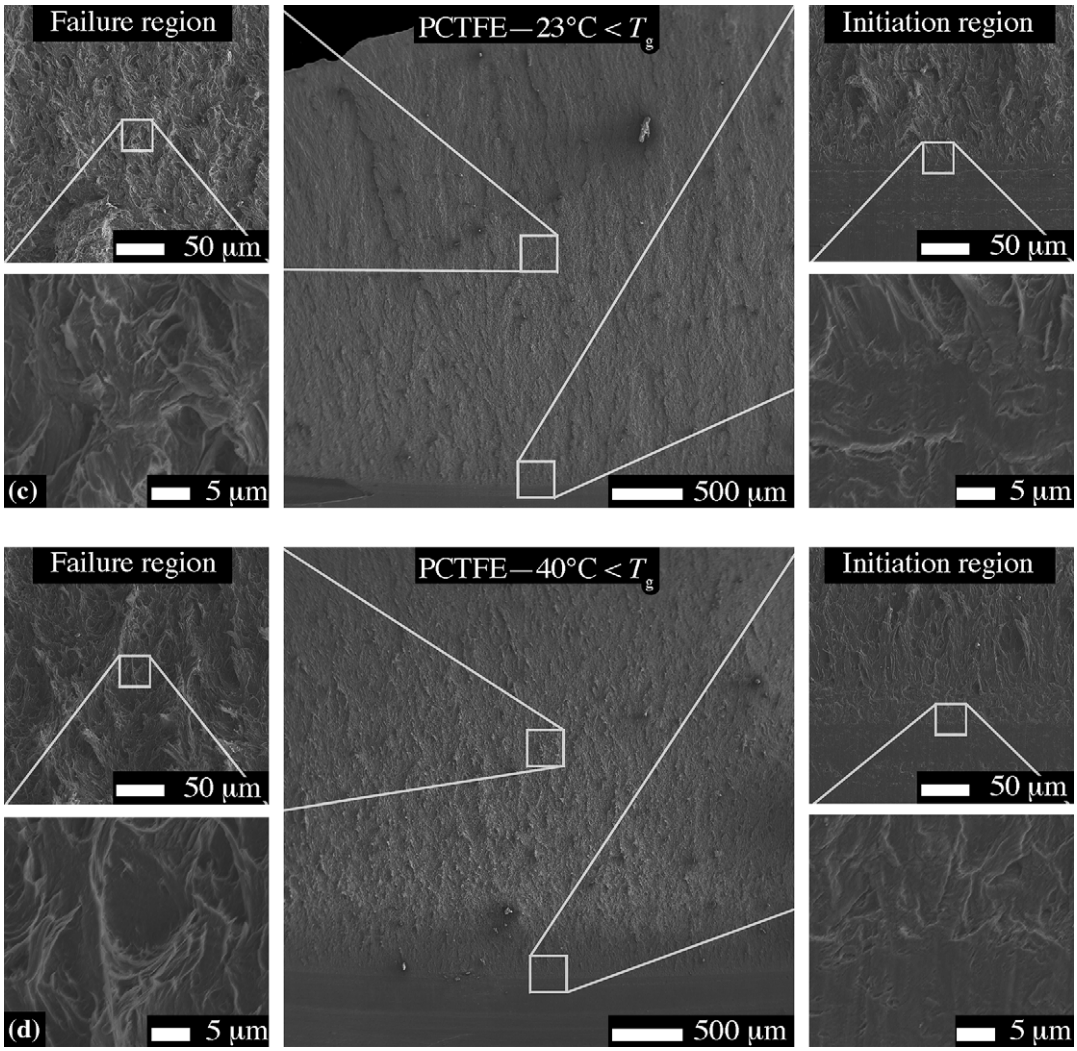

Fig. 12. (*continued*)

micrographs: (1) crazing below T_g (as shown in Fig. 12) and (2) ductile failure with significant localized deformation and tufted drawing of PCTFE above T_g (as shown in Fig. 13). The fracture morphology exhibits relatively little temperature dependence below T_g, with a subtle increase in the relevant craze length-scale. At none of the temperatures studied does PCTFE exhibit a distinct transition in fracture plane morphology associated with a plastic zone at the crack tip as observed for polymers such as epoxy [49] and PEEK [50]. In addition to the surface craze morphology observed in the SEM micrographs, stress whitening associated with a craze zone is observed to extend far in advance of the crack tip. The depth profiles of the craze zone along the center plane of the samples are shown in Fig. 14. The depth at 0.2 mm from the crack tip is indicated to correspond with the J–R initiation criteria. Below T_g, the craze depth increases from being negligible at −50 °C to 0.3 mm at 40 °C. Consistent with the dramatic increase and drop of J_{IC} as the temperature passes through T_g the craze depth increases to 0.6 mm and then decreases to less than 0.03 mm. In addition to the change in depth of this zone, the morphology changes from classic crazing to drawing. This is particularly clear in the tufted morphology at 80 °C in Fig. 13b and in the side view of Fig. 14. It is worth noting that the temperatures for dominant craze behavior is bounded by the γ and β (T_g) transitions from DMA, with nominal crazing below γ and tufting above β.

3.5. Taylor impact

Taylor impact shots were carried out at room temperature (23 °C) and at 60 °C to understand the ductile brittle transition in PCTFE. Fig. 15 shows a velocity versus mode plot for PCTFE at 23 and 60 °C. Three modes were observed; ductile, where other than permanent deformation and stress whitening no fractures occurred; cracking, where the center of the impact zone exhibited one or more cracks but the sample remained fully intact; and brittle, where the sample fractured into two or more separate pieces. At room temperature the behavior spanned a relatively large range of velocities. The first brittle event occurred at only 170 m s^{-1} while one sample deformed in a ductile manner from 197 m s^{-1}. Examples of two of the failure modes and the spread in response with respect to

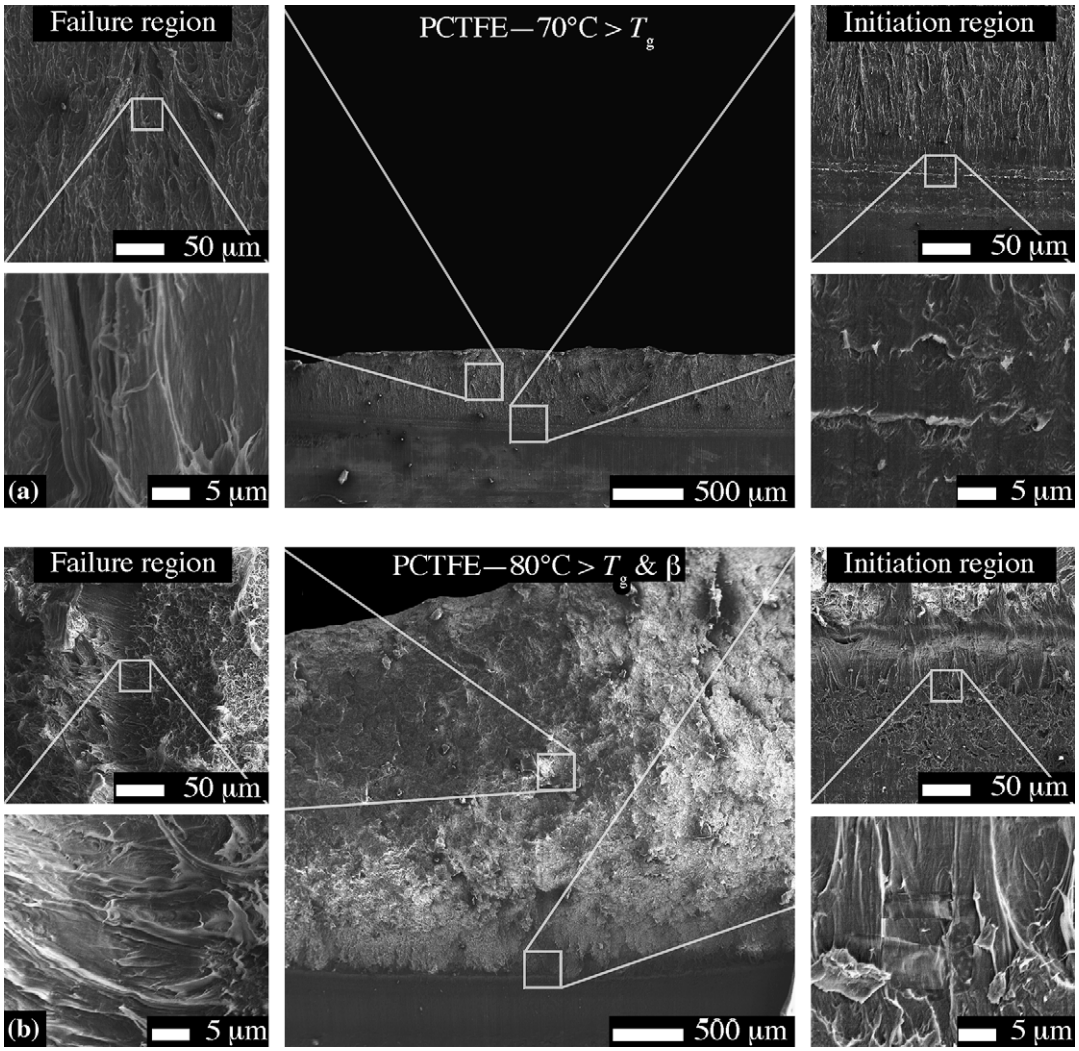

Fig. 13. SEM micrographs of the fracture plane morphology for PCTFE above the glass transition temperature at 0.025 mm s^{-1} loading rate. Note: crack propagation is from bottom to top.

velocity can be seen in Fig. 16. One sample is shown that was shot at 197 m s^{-1} and retrieved with the common three-diameter ductile deformation pattern, while another sample fired at 4 m s^{-1} slower shows a brittle response. The sample fired at 202 m s^{-1} shows extensive fragmentation. In contrast to 23 °C, at 60 °C a smooth monotonic transition between ductile, cracking, and brittle response occurs over a velocity range of only 8 m s^{-1}.

4. Discussion

4.1. Rate dependence of T_g

The glass transition temperature measured for PCTFE is markedly different for DSC (47 °C) and DMA methods (63–79 °C for strain rates of 0.1–100 rad s^{-1} based on the break in slope of G'). This discrepancy is commonly found in many polymers. Moreover, it is exacerbated by the existence of three ways to estimate T_g from a DMA trace [54]. We have previously reported on the observed increase in T_g with strain rate for a range of fluoropolymers [6] based on max flow stress for bulk quasistatic and split-Hopkinson pressure bar measurements. The max flow stress was plotted as a function of temperature for multiple strain rates, similar to the results shown for PCTFE in Fig. 17. Flow stress is used, rather than modulus as in the case of DMA experiments, due to the ringing-up – i.e., the time required for the sample to reach stress state equilibrium, see Gray [43] – in the SHPB experiments obscuring the modulus at higher rates. The relationship between flow stress and temperature has been empirically shown to be linear in the absence of transitions in the deformation mechanisms. As shown in Fig. 18, PCTFE exhibits subtle transitions associated with the T_g at 47 °C, with the low rate tensile and compressive data transitioning at the thermal T_g. The high-rate transition appears to increase to 90 °C.

In some polymers the yield strength dramatically increases at strain rates between 100 and 1000 s^{-1}, which has been attributed to the strain-rate dependence of β and γ relaxations seen in DMA analysis [55,56]. As the strain rate increases,

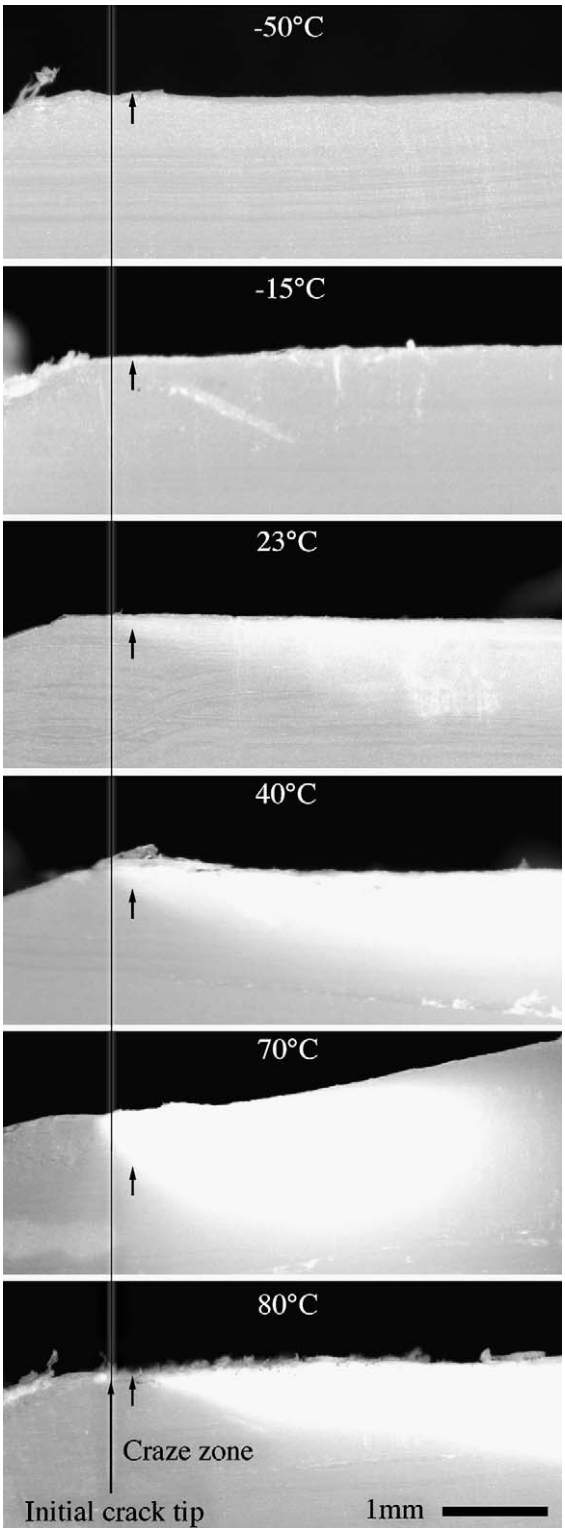

Fig. 14. The depth profiles of the craze zone imaged as stress whitening by optical microscopy along the center plane of the samples as a function of temperature. Note: crack propagation is from left to right.

the temperature of the relaxations also increases. In polycarbonate and PVDF extrapolation has shown that these relaxations reach room temperature at strain rates similar to those where a rapid increase in yield stress occurs. The clear

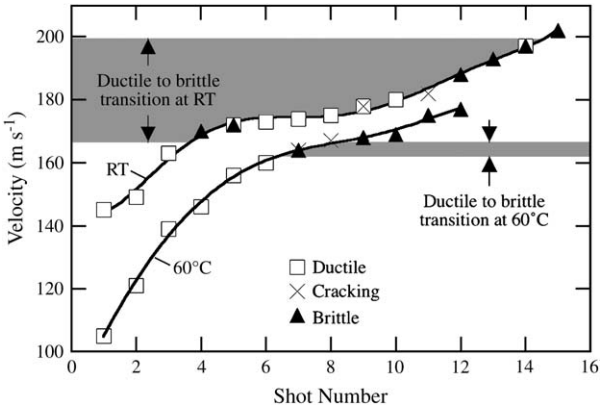

Fig. 15. The transition from ductile-to-brittle response in PCTFE at 23 and 60 °C in the Taylor's test. The solid lines are to aid the eye.

frequency dependence of the γ relaxation in PCTFE can be seen from Fig. 8. The DMA deformation profile was sinusoidal with a maximum strain of 0.1%. The maximum strain rate during a loading cycle of DMA measurement can therefore be calculated and extrapolated in a manner similar to Siviour et al. [55]. From this analysis the γ relaxation peak would be expected to reach room temperature at approximately 300 s^{-1} in this case. However, it can be seen from Fig. 18 that for the case of PCTFE, a marked deviation from the yield strength trend does not occur close to this rate. A possibly related observation is that most polymers have a linear dependence of yield stress to logarithmically plotted strain rate up to some limiting rate [40–42,55,57], again this is not the case with PCTFE.

In Fig. 18 the maximum stress associated with yield is plotted as a function of strain rate for tension and compression. Over seven decades of compressive strain-rate an empirical smooth power-law curve is seen to provide an accurate fit to the data. This is in contrast to many other polymers where a bi-linear relationship is observed [40–42,55,56]. The tension curve appears to follow the same trend but with a systematically lower stress and a diverging gradient. The single high-rate (725 s^{-1}) tensile data point is from a pair of tensile Hopkinson bar experiments using the geometry and apparatus described in Ref. [2]. Obtaining stress equilibrium prior to material localization in such experiments is problematic and so the stress value has a possible error associated with it. If equilibrium is truly achieved before necking the data are accurate, if not the actual value would likely be higher. Nevertheless, the point is included for reference.

4.2. Comparison to the literature

The bulk mechanical response of PCTFE has received very limited attention in the literature. The two noteworthy investigations of the tensile behavior of PCTFE were performed by Imai and Brown [22] and Hartmann and Lee [25]. Imai's data [22] are on uncharacterized PCTFE (Kel-F 81 Grade 3) from 3M Co. However, in subsequent papers on Kel-F 800 [23,24] they specify pressing by the Fluorocarbon Company

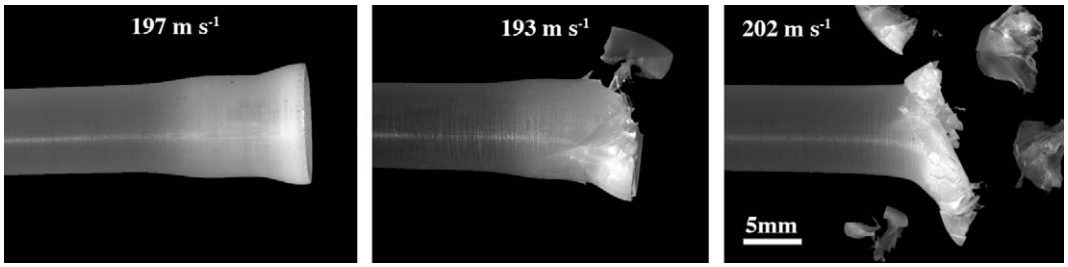

Fig. 16. A micrograph of three-post test Taylor cylinders fired at 23 °C. The sample fired at 197 m s^{-1} suffered less damage than the one fired at 193 m s^{-1}. The sample fired at 202 m s^{-1} exhibits extensive shattering.

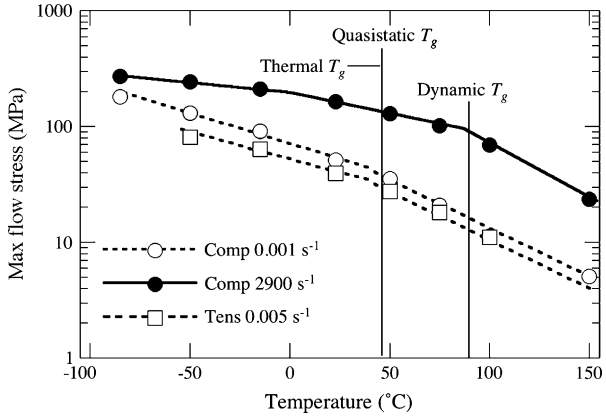

Fig. 17. Yield strength versus temperature in tension and compression. The point T_g is designated by the break in slope of the bi-linear relationship.

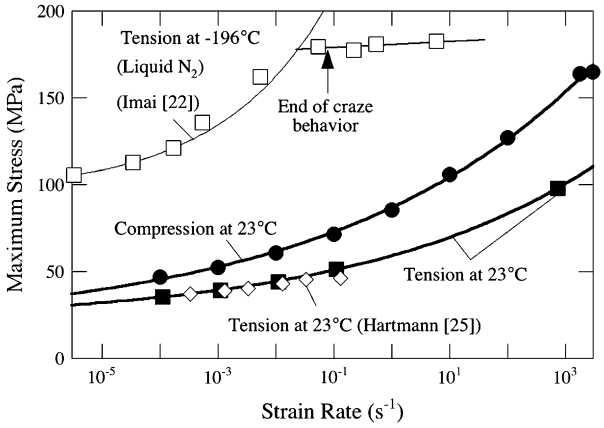

Fig. 18. The maximum stress associated with yield as a function of strain rate at 23 ± 1 °C. The regression fitted curves are to an empirical power-law equation of the form $y = a + bx^c$. In compression $a = 16.6$, $b = 70.2$, and $c = 0.0965$ and in tension $a = 20.7$, $b = 38.3$, and $c = 0.106$.

with a water quench from 300 °C. This would suggest a relatively low crystallinity. Hartmann's data [25] are on commercially obtained sheet of PCTFE (Kel-F) from 3M Co. with a density of 2139 kg m^{-3} and crystallinity of 58% (calculated from the equation proposed by Hoffman and Weeks [28]). Imai's [22] rate data were obtained at liquid nitrogen conditions, and are plotted in Fig. 18. As can be seen, even at this greatly depressed temperature the standard linear relationship between yield and log strain rate does not hold true for this material. Moreover, the observed transition at this temperature associated with the interruption of craze formation in PCTFE leads to a decreased slope at high rate contrary to the standard increase. Hartmann's [25] rate data obtained at room temperature show excellent agreement with the current data despite its lower crystallinity[3] (Fig. 18). Comparison of the temperature dependence of the current PCTFE and that of Hartmann and Lee [25] is shown in Figs. 19 and 20. The flow stress shows excellent agreement within the scatter of Hartmann's data, with both data sets exhibiting the same break at T_g. The modulus in the current work is slightly higher than that of Hartmann, although this is likely due to the difference in crystallinity. Both modulus data sets exhibit the same break at T_g.

[3] Hoffman and Weeks [28] only provided crystallinity data for their material based on the density method. Using Hoffman's proposed values for amorphous and crystalline PCTFEs the crystallinity of the material in the current work based on density is 75%.

4.3. Dynamic ductile-to-brittle transitions

Rae et al. [4] previously employed the Taylor test to investigate the dynamic ductile-to-brittle transitions in PTFE. The transition velocity for a range of temperatures was shown by Rae et al. to correspond to the pressure where PTFE undergoes a crystalline phase transition from a ductile-to-brittle phase. The range of velocities over which the transition from ductile-to-brittle occurred in PTFE was less than 2 m s^{-1} at all but the highest temperature where the range was less than 4 m s^{-1}. The wide

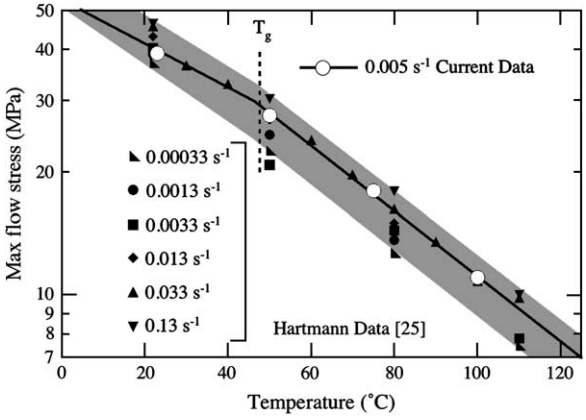

Fig. 19. Yield strength versus temperature in tension comparing the current data with Hartmann and Lee [25].

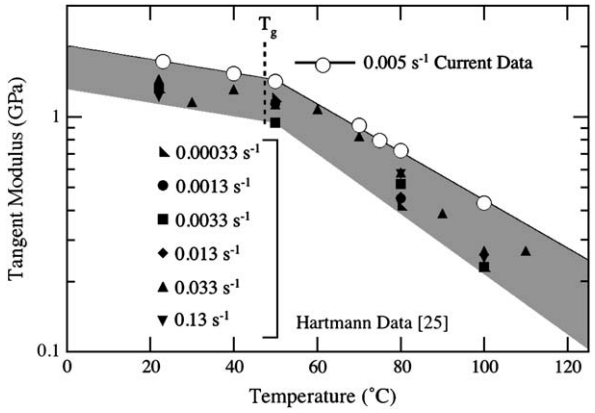

Fig. 20. Tangent modulus versus temperature in tension comparing the current data with Hartmann and Lee [25].

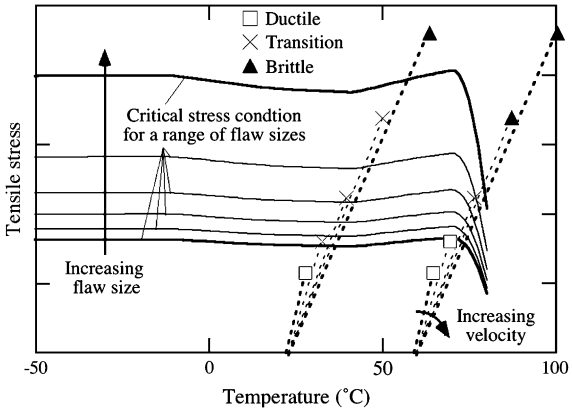

Fig. 21. Critical failure stress and impact loading path in stress temperature space for a range of flaw sizes, impact velocities, and initial temperatures.

range of the transition velocity over 34 m s^{-1} from ductile-to-brittle in PCTFE at room temperature was used to illustrate the response of a polymer to Taylor impact tests in the absence of a phase transition. This wide range in transition velocities has been observed to be common for a range of polymers including Kel-F 800 [58] and PEEK [50,59], as well as metals (i.e., 39 m s^{-1} in AF1420 steel) [60]. It is therefore interesting that at 60 °C PCTFE exhibits a smooth monotonic transition between ductile, cracking, and brittle response over a velocity range of only 8 m s^{-1}.

The reduced range of velocities for the ductile-to-brittle transition at the high temperature can qualitatively be explained using the fracture toughness data presented above. While the fracture toughness of polymers is expected to be rate dependent, obtaining fracture toughness at the rates relevant to the Taylor test ($>10^4$ s^{-1}) is not practicable. Therefore, in applying a fracture mechanics approach to estimate crack propagation we assume that the form of fracture toughness and elastic modulus dependence on temperature remains correct [61]. Following Griffith [62], a sharp-ended flaw of characteristic length $2a$ will propagate when the applied far field tensile stress exceeds a critical value defined as

$$\sigma_C \geq m\sqrt{\frac{E\gamma}{a}} = m\sqrt{\frac{EJ_{IC}}{a}}, \tag{6}$$

where m is a constant of order 1 defining the flaw geometry relative to the loading condition and γ is the free surface energy, which is more accurately captured by the materials' fracture toughness. A schematic plot of Eq. (6) is given in Fig. 21 for a range of flaw sizes, with the largest flaw six times the size of the smallest. As can be seen, for a given flaw size, the critical stress is almost constant for all temperatures above the T_g at which point the critical stress drops precipitously. The stress values are not given as m will take on a range of values depending on the orientation and location of the critical flaw in the Taylor cylinder, the relevant range of flaw sizes is not known, and the E and J_{IC} values used are only relative. Moreover, the actual values of stress are not needed for this discussion.

The kinetic energy of a Taylor sample – which will be partitioned as elastic deformation, plastic deformation, heat, and crack growth – scales with the square of the projectile velocity, U^2. To first-order the increase in both the sample temperature [63] and the sample strain [64] scale with U^2 and the stress scales to with strain. Assuming no failure, the end states (maximum compression, prior to rebound) of Taylor samples at five velocities are shown schematically in Fig. 21 for initial temperatures of 23 and 60 °C. The combined effects of shock heating and large-strain heating in PCTFE for a range of velocities investigated are expected to be on the order of 30 °C. For the purposes of this discussion only the six flaw sizes shown are considered to be relevant. Therefore, it is clear that with an initial room temperature condition the slowest impact velocity will never drive a crack and the fastest impact velocity will always drive a crack. At the interim velocities, however, whether or not the crack will propagate will depend on the size of the flaws present. In this regime a sample with a slower impact velocity but with a large flaw will fail in a brittle fashion, while a sample with a faster impact velocity but with a small flaw will deform in a ductile fashion. It is also possible in this regime that the stress required to propagate a crack will not be reached until late in the impact event. The combined local unloading due to crack initiation and bulk unloading due to end of the impact event will be expected to result in the formation of cracks without full brittle fracture. On the other hand, when the initial temperature is sufficiently elevated (60 °C) the loading path in stress–temperature space for the same velocities will transect the critical stress curves in the region of precipitous drop above T_g rather than the constant region. Therefore, of the five velocities considered the two slowest impact velocities will never drive a crack and the two fastest impact velocities will always drive a crack. At only one of the interim velocity is crack growth dependent on the flaw size. This would in turn result in the dramatic decrease in the observed range of velocities for the ductile-to-brittle transition.

5. Conclusions

A broad study of the influence of temperature and strain rate on the constitutive and damage responses of PCTFE has

been performed. There is a clear tension–compression asymmetry with the tensile yield being as much as 30% less than in compression. The stress–strain response exhibits a strong dependence on both temperature and rate. However, PCTFE does not exhibit the classic transition in rate dependence between 100 and 1000 s^{-1} as seen in many polymers. In tension localized necking dominates yield above the γ transition. The fracture toughness increases slightly with temperature below T_g, with crazing being the dominant fracture morphology particularly above the β transition. Above T_g, the fracture toughness increases significantly followed by a precipitous drop, with crazing giving way to a tufted morphology. Three modes were observed under Taylor impact loading; ductile, where other than permanent deformation and stress whitening no fractures occurred; cracking, where the center of the impact zone exhibited one or several cracks but the sample remained fully intact; and brittle, where the sample fractured into two or more pieces. At room temperature this transition spans a 34 $m\,s^{-1}$ range of velocities, while at 60 °C the velocity range is only 8 $m\,s^{-1}$ due to the drop in fracture toughness at the elevated temperature.

Acknowledgements

This research was supported under the auspices of the US Department of Energy operated by the Los Alamos National Security LLC and the Joint DoD/DOE Munitions Program. B. Clements is the project leader.

References

[1] Bunn CW, Howells ER. Nature 1954;174(4429):549.
[2] Rae PJ, Brown EN. Polymer 2005;46(19):8128.
[3] Rae PJ, Dattelbaum DM. Polymer 2004;45(22):7615.
[4] Rae PJ, Brown EN, Clements BE, Dattelbaum DM. J Appl Phys 2005; 98(6):063521.
[5] Brown EN, Dattelbaum DM. Polymer 2005;46(9):3056.
[6] Brown EN, Rae PJ, Gray GT III. J Phys IV France 2006;134:935.
[7] Brown EN, Rae PJ, Orler EB, Gray III GT, Dattelbaum DM. Mater Sci Eng C 2006;26:1338–43.
[8] Brown EN, Clausen B, Brown DW. J Neutron Res, in press.
[9] Brown EN, Rae PJ, Liu C. Mater Sci Eng A, submitted for publication.
[10] Brown EN, Rae PJ, Trujillo CP, Dattelbaum DM, Gray GT III, Bourne NK. In: Proceedings of the APS shock compression of condensed matter conference, in press.
[11] Bourne NK, Gray III GT. J Appl Phys 2003;93(11):8966.
[12] Robbins AL, Sheffield SA, Alcon RR. In: Proceedings of the APS shock compression of condensed matter conference, vol. 706; 2004. p. 675.
[13] Champion AR. J Appl Phys 1971;42:5546–50.
[14] Nagao H, Matsuda A, Nakamura KG, Kondo K. Appl Phys Lett 2003;83: 249–50.
[15] King RF, Tabor D. Proc Phys Soc B 1953;66:728.
[16] Longhenry JL, Love BJ, Murthy NS. J Mater Sci 1997;32(9):2283.
[17] Love BJ, Cherry K, Longhenry JL, Murthy NS, Bednarczyk C. J Mater Sci Lett 1998;17(19):1681.
[18] Iyer N, Saka N, Chun JH. IEEE Trans Semicond Manuf 2001;14(2):85.
[19] Subrahmanyan S, Dillard JG, Love BJ, Romand M, Charbonnier M. J Vac Sci Technol 2002;20(3):707.
[20] McCrum NG. J Polym Sci 1962;60(169):S3.
[21] Gray RW, McCrum NG. J Polym Sci B 1966;4(9):639.
[22] Imai Y, Brown N. J Polym Sci 1976;14(4):723.
[23] Imai Y, Brown N. Polymer 1977;18(3):298.
[24] Brown N, Metzger BD. J Appl Phys 1977;48(10):4109.
[25] Hartmann B, Lee GF. Polym Eng Sci 1991;31(4):231.
[26] Shoemaker M, Sterling P. In: International symposium for testing and failure analysis proceeding; 1986. p. 251.
[27] Mencik Z. J Polym Sci 1973;11:1585.
[28] Hoffman JD, Weeks JJ. J Res Natl Inst Stand Technol 1958;60(5): 465.
[29] Privalko VP, Tarara AM, Bezruk LI, Veselov OI, Korab GN. Polym Sci USSR 1985;27(3):642.
[30] Khanna YP, Kumar R. Polymer 1991;32:2010.
[31] Chang SS, Weeks JJ. J Res Natl Inst Stand Technol 1992;97:341.
[32] Polychlorotrifluoroethylene, Kel F. In: Marsh SP, editor. LASL shock Hugoniot data. University of California Press, ISBN 0-520-04007-4; 1980. p. 434–5.
[33] Anderson MU. In: Schmidt, Dick, Forbes, Tasker, editors. Proceedings of the APS shock compression of condensed matter conference; 1991. p. 875–8.
[34] Sheffield SA, Alcon RR. In: Schmidt, Dick, Forbes, Tasker, editors. Proceedings of the APS shock compression of condensed matter conference; 1991. p. 909–12.
[35] Samara GA, Fritz IJ. J Polym Sci Polym Lett 1975;93–100.
[36] Miller RL. In: Brandrup J, Immergut EH, editors. Polymer handbook. New York: Wiley; 1975.
[37] Bueche AM. J Am Chem Soc 1952;74:65.
[38] Cady WE, Caley LE. Properties of Kel-800 polymer. Lawrence Livermore laboratory report UCRL-52301; July 21 1977.
[39] Murthy NS, Khanna YP, Signorelli AJ. Polym Eng Sci 1994;36:1254.
[40] Walley SM, Field JE, Pope PH, Safford NA. Philos Trans R Soc London Ser A 1989;328(1597):1.
[41] Walley SM, Field JE, Pope PH, Safford NA. J Phys III 1991;1(12):1889.
[42] Walley SM, Field JE, Safford NA. J Phys III France 1991;1(C3): 185–90.
[43] Gray III GT. Classic split Hopkinson pressure bar testing. In: ASM handbook. Mechanical testing and evaluation, vol. 8. ASM; 2000. p. 462.
[44] Panametrics. Ultrasonic technical notes, www.panametrics.com; 2001. p. 32–40.
[45] Landes JD, Herrera R. Int J Fract 1988;36(1):r9.
[46] Morhain C, Velasco JI. J Mater Sci 2001;36(6):1487.
[47] Landes JD. J Test Eval 2003;31:1.
[48] Joyce JA. Polym Eng Sci 2003;43(10):1702.
[49] Brown EN, White SR, Sottos NR. J Mater Sci 2004;35(5):1703.
[50] Rae PJ, Brown EN, Orler EB. Polymer, submitted for publication.
[51] McCrum NM, Read BE, Williams G. Anelastic and dielectric effects in polymeric solids. New York: Dover Publications; 1967. p. 464–77.
[52] Dick JJ, Martinez AR, Hixson RX. Plane impact response of PBX 9501 and its constituents below 2 GPa. LANL report LA-13426-MS; April 1998.
[53] Kwan SF, Chen FC, Choy CL. Polymer 1975;16(7):481.
[54] Menar KP. Dynamic mechanical analysis: a practical introduction. CRC Press, ISBN 0-8493-8688-8; 1999.
[55] Siviour CR, Walley SM, Proud WG, Field JE. Polymer 2005;46:12546.
[56] Richton J, Ahzi S, Vecchio KS, Jiang FC, Adharapurapu RR. Int J Solids Struct 2006;43:2318.
[57] Hamdan S, Swallowe GM. J Mater Sci 1996;31:1415.
[58] Rae Kel-F 800. Unpublished data; 2006.
[59] Millett JCF, Bourne NK, Stevens GS. Int J Impact Eng 2006;32(7):1086.
[60] Gilmore MR, Foster JC, Wilson LL. In: Proceedings of the APS shock compression of condensed matter conference, vol. 620; 2002. p. 519.
[61] Willmott GR, Radford DD. J Appl Phys 2005;97(9):093522.
[62] Griffith AA. Philos Trans R Soc London Ser A 1920;221:163.
[63] Celentano DJ. J Appl Phys 2002;91(6):3675.
[64] Taylor G. Proc R Soc London Ser A 1948;194(1038):289–99.